COMMUNICATION

Check for updates

Protector-free, non-plasmonic silver quantum clusters by femtosecond pulse laser irradiation: *in situ* binding on nanocellulose filaments for improved catalytic activity and cycling performance

Toyoko Imae, [ID] *[a] Shambel Abate Marye,[a] Ling Wang[b] and Orlando J. Rojas [ID] *[bcde]

This study introduces a new, facile method to synthesize silver clusters from aqueous silver ion solution by using high intensity femtosecond pulse laser irradiation. The particles obtained in the absence of reducing or capping agents are 1–17 nm in size and presented quantum properties, as characterized by fluorescence, but did not exhibit plasmon signals, which is not a common characteristic of conventional silver nanoparticles. In a further development, small silver quantum clusters (~1 nm) were bound *in situ* to wet-spun filaments of cellulose nanofibrils by pulsed laser irradiation. The obtained hybrid filaments as well as free silver quantum clusters revealed a catalytic activity remarkably higher than that of free gold quantum clusters; moreover, the hybrid filaments were found to show improved stability and cycling performance for silver-based catalysis. The present results indicate the potential of femtosecond laser irradiation to generate clusters as well as hybrid systems with excellent performance and reactivity.

New concepts

Atomic clusters have a unique character, setting them apart from nano-particles, but their activity has not been experimentally validated due to synthesis challenges. Moreover, the stabilizers used in the synthesis of clusters modify their properties, which is not the case of the bare counterparts (unprotected clusters, produced in the absence of stabilizers). Hence, unprotected clusters emerge as attractive choices for catalysis and beyond. This is central to this work where Ag clusters, ~1 nm, were synthesized using a physical protocol based on femtosecond pulse laser irradiation, using no chemical stabilizers. This bottom-up procedure imparted properties similar to those of Au quantum clusters, including fluorescence (T. Imae, A. Rahmawati, A. M. Berhe, M. A. Kebede, *ACS Appl. Nano Mater.*, **2022**, 5(11), 16842–16852) but with no plasmonic effects (occurred for Ag nanoparticles produced by chemical synthesis in solution). A solid support for the Ag clusters was further tested, in the form of wet-spun filaments made from cellulose nanofibrils. As such, the clusters were conveniently synthesized and attached *in situ* on formed filaments that demonstrated catalytic activity, comparable to that of the free Ag clusters. Moreover, the hybrid filaments exhibited better stability and cycling performance, adding new insights to the area of atomic clusters, properties and applications.

1. Introduction

The synthesis, characterization, and application of metal clusters have received increased attention over recent years.[1] Electrically conductive bulk metals are known as good light reflectors due to the free, delocalized electrons of the conduction band. In contrast, metal nanoparticles, including silver, gold, and copper, exhibit intense color owing to surface plasmon resonance (SPR). This feature is the result of collective resonant oscillation of conduction electrons interacting with incident light photons. Metal clusters are composed of metal particles with sizes < 1 nm, comparable to the de Broglie wavelength of an electron. Such metal clusters might exhibit different properties but do not exhibit plasmon effects; hence, as far as their properties and sizes, they are classified between metal atoms and plasmon nanoparticles.[2] Due to the severe quantum size confinement, metal clusters exhibit discrete levels of energy (discontinuous band structure) and electronic transition, resulting in intense light absorption and emission.

The described major category of quantum clusters, with a number of atoms ranging from a few to a finite number, is of great interest for application in advanced technologies. In fact, the past few years have seen major advances in atomically

[a] Graduate Institute of Applied Science and Technology, National Taiwan University of Science and Technology, Taipei 10607, Taiwan.
E-mail: imae@mail.ntust.edu.tw

[b] Department of Bioproducts and Biosystems, School of Chemical Engineering, Aalto University, 00076, Finland

[c] Bioproducts Institute, Department of Chemical & Biological Engineering, The University of British Columbia, Vancouver, BC V6T 1Z3, Canada.
E-mail: orlando.rojas@ubc.ca

[d] Department of Chemistry, 2036 Main Mall. Vancouver, The University of British Columbia, Vancouver, BC V6T 1Z1, Canada

[e] Department of Wood Science, The University of British Columbia, 2900-2424 Main Mall, Vancouver, BC V6T 1Z4, Canada

precise metal clusters, opening up new directions in nanoscience.[3] Especially, great interest in silver and gold clusters has emerged due to their inherent physical, chemical, optical, and electrical characteristics compared to their bulk counterpart.[2] Applications of metal clusters include catalysts,[4] sensors,[5] antibacterial agents,[6] and bioimaging[5] devices as well as nanoelectronic components.[7] Silver and gold clusters have high catalytic activity, such as for selective reduction of oxygen,[8] NO_x,[9] and 4-nitrophenol.[10] Of significance to the present study is the expectation that capping-free, bare metal clusters are more efficient catalysts because the absence of the organic components allows for better access to reactants. An example is that of silver clusters protected by co-polymer ligands, which show a decreased catalytic activity for the reduction of 4-nitrophenol.[11]

Metal clusters can be prepared using physical and chemical synthesis, including those mediated by inverse micelle,[12] chemical reduction,[13] microwave-assisted,[14] and laser irradiation[15] systems. In such processes, protectors are utilized as stabilizers and size-controllers, e.g., to produce small metal clusters and to prevent their aggregation. However, protectors almost inevitably affect the intrinsic characteristics of metal clusters. To obtain protector-free clusters, additional treatments have been considered, for instance, UV-ozone treatment,[16] thermal annealing,[17] and acetic acid washing.[18] These post-treatments require high temperatures or extreme conditions, leading to variations in their particle size and shape. Therefore, there is a demand for methods using mild conditions capable of synthesizing protector-free clusters.

Herein, we considered a bottom-up synthesis by the irradiation of femtosecond pulse laser to produce protector-free particles. This synthesis benefits from products (OH*, H* and e_{aq}^- species) affecting the optical decomposition of water under the irradiation. Zinc oxide and copper oxide particles have been synthesized by the reaction of OH* with metal ions and the dehydration in water during the femtosecond pulse laser irradiation.[19,20] Protector-free clusters and nanoparticles produced from this physical procedure provide higher fluorescence, a larger bandgap, and more effective catalytic activity compared to nanoparticles prepared from conventional chemical reactions.[21] Au clusters have been generated through the process of the reduction reaction of tetrachloroaurate ions by e_{aq}^-.[22] They emit fluorescence, which is characteristic of quantum clusters, and nanoparticles larger than 5 nm exhibit both quantum and plasmonic properties,[22,23] where Pt particles are always small (<2 nm) and show neither quantum nor plasmon character. Thus, the characteristics of atomic clusters depend on the metal species, as defined by the given precursors.

Silver particles were synthesized using short-time femtosecond laser irradiation with neither stabilizing nor reducing agents. The process only relied on the metal precursor, leading to clusters with bare, highly active surfaces. The presented direct synthesis method achieved uncapped (protector-free) silver clusters exhibiting quantum properties, which is in contrast to their Au counterparts. The duration of femtosecond pulse laser irradiation, the precursor concentration, and the type of target metal are shown to influence the development of

the metal particles. Thereafter, size-dependent chemical, physical, electrical, optical, and catalytic properties were assessed. The Ag clusters were compared with conventional Ag nanoparticles as well as Au clusters and nanoparticles.

2. Experimental

2.1. Materials and methods

Silver nitrate ($AgNO_3$, 99.9%) was obtained from Sigma Aldrich Co., USA. Sodium borohydride ($NaBH_4$), 4-nitrophenol ($C_6H_5NO_3$), 2-propanol (C_3H_8O), and 2,2,6,6-tetramethyl-1-piperdinyloxy free radical (TEMPO) (98+%) were purchased from Acros organics, USA. 5,5-Dimethyl-1-pyrroline-N-oxide (DMPO, 98%) was a product of Columbia (USA). All chemicals were used without further purification. Ultra-pure (Millipore Milli-Q) water with a resistivity of 18.2 MΩ cm was used throughout the whole solution preparation. Indium-tin oxide (ITO) glass was purchased from Aim core Technology, Taiwan.

Femtosecond laser (Kokyo Inc., Japan, wavelength: 1550 nm) was generated by pulse laser amplification.[19] The power output of the laser was measured with a laser power energy meter (Solope, Gentec-EO, Canada) and found to be 47 mW. An infrared sensor card (F-IRC2, Newport, USA, wavelength: 0.8–1.7 μm) was used to point out or locate near-infrared radiation of an invisible laser light. An atomic force microscope (AFM, Veeco Instruments Inc., USA) was used to observe the specimens deposited and dried on a freshly cleaved mica surface. X-Ray photoelectron spectroscopy (XPS) was carried out on a VG Scientific ESCALAB 250, England. Ultraviolet (UV)-visible absorption spectra (JASCO V-670, Japan) and fluorescence spectra (Hitachi F-7000, Japan) were measured using a 2 mm quartz cuvette. A field emission gun transmission electron microscope (FETEM, FEI Tecnai™ G2 F-30 S-TWIN, Philips, USA) was operated at a 200 kV accelerating voltage.

2.2. Cellulose nanofibrils (CNF) and filament spinning

Cellulose nanofibrils (CNF) were prepared according to the literature.[24] Briefly, never dried bleached birch fibers were first TEMPO-oxidized and processed via high-pressure microfluidization. The obtained aqueous suspension contained cellulose nanofibrils (1.6 wt% solids) with a carboxylic group content of 0.6 mmol g^{-1}. Wet spinning was used to process the CNF suspension into filaments. CNF was loaded into a 50-ml syringe and extruded (0.64 m min^{-1}) into a bath containing HCl solution (pH 2), used as an antisolvent. The coagulated hydrogel fibers were continuously collected on a winder (22 cm diameter) at a 3.6 m min^{-1} rate. Finally, the filaments were dried overnight.

2.3. Synthesis of silver particles via femtosecond laser

Silver nitrate (0.849 mg, 1 mM) was dissolved in water by sonication for 5 to 10 min. A solution (2 ml) was placed into a quartz cuvette (10-mm path length) with a cleaved mica substrate on a magnetic metal plate for AFM measurement. For the in situ deposition of silver particles on the CNF filaments, the latter were immersed into the reaction cuvette

Fig. 1 (A) AFM images and histograms of silver particles synthesized by laser irradiation for (a) 3, (b) 10 and (c) 60 min using 1 mM AgNO$_3$ solution. (B) Average AFM heights of silver particles *versus* irradiation time. The inset indicates the average height *versus* irradiation time, from 1 min to 5 min. (C) AFM images and histogram distributions of silver particles at 2 min irradiation for AgNO$_3$ concentrations of (a) 3, (b) 10, and (c) 20 mM. (D) Average AFM height of silver particles as a function of precursor concentration. (E) TEM images, size histograms and (F) HR-TEM images of silver particles produced at (a) 2, (b) 3, and (c) 30 min laser irradiation.

for replacing the mica substrate. The femtosecond laser beam was irradiated on the quartz cuvette perpendicular to its side surface. All the processes were carried out in the dark and at room temperature (~ 25 °C).

2.4. Quantum yield of silver particles

The procedure requires a standard sample with a known quantum efficiency and the optical properties closely related to those of the testing compound. Eqn (1) was used to determine the quantum efficiency (Φ_X):[25]

$$\Phi_X = \Phi_R \cdot \frac{A_R}{A_X} \cdot \frac{E_X}{E_R} \cdot \frac{I_R}{I_X} \cdot \frac{n_X^2}{n_R^2} \qquad (1)$$

where Φ is the quantum yield, A is the absorbance, E is the emission intensity, I is the relative intensity of the exiting light and n is the average refractive index of the solution. The subscripts R and X refer to a standard and the tested compound, respectively.

2.5. Catalytic reduction of 4-nitrophenol

Catalytic reduction was studied by mixing aqueous 4-nitrophenol (0.1 mM, 1.5 ml) solution with aqueous sodium borohydride (0.1 M, 1.5 ml) in a quartz cuvette (1 cm path length). Silver particles were added (0.52, 0.74, and 0.86 mg, respectively, for 1-, 5- and 10-min laser-irradiated particles). Alternatively, CNF filaments carrying silver clusters were used. The reactions were monitored on a UV-visible absorption spectrophotometer at room temperature (~ 25 °C). For comparison, the catalytic reaction was also performed with gold catalysts using the same conditions as those used for silver. The used amounts were 0.36, 0.5, and 0.76 mg for gold materials at laser irradiation times of 1, 5 and 10 min, respectively, which were prepared from a 1 mM solution.

3. Results and discussion

3.1. Synthesis of silver particles

Synthesis of silver particles by femtosecond pulse laser irradiation was performed in aqueous media, with neither reducing nor stabilizing agents. Fig. 1A shows the AFM images and height distribution histogram of the silver particles synthesized from aqueous 1 mM AgNO$_3$ solution using different irradiation times. The AFM images showed silver particles as small dots that were well distributed. The mean vertical height of the particles calculated from AFM profiles were 2.5 ± 0.6, 8.8 ± 2.8 and 16.9 ± 12.6 nm corresponding to 3-, 10- and 60-min irradiation times, respectively. Similar AFM observations were performed for products using other irradiation times, and the height values are listed in Table 1 and plotted in Fig. 1B against the femtosecond laser irradiation time. The particle height increased with irradiation time from 0.9 nm at 1 min to 16.9 nm at 60 min. Although most of the histograms were unimodal, irradiation for 45 and 60 min produced larger particles, 35 and 40 nm at less than 4 number% (Table 1).

AFM images were also obtained for particles synthesized after 2-min irradiation at different silver precursor concentrations

Table 1 Average height of silver particles calculated from AFM section analyses

Silver ion concentration (mM)	Irradiation time (min)	Average AFM particle height (nm)
1	1	0.9 ± 0.3
1	2	1.8 ± 0.8
1	3	2.5 ± 0.6
1	5	6.8 ± 1.9
1	10	8.8 ± 2.8
1	20	11.6 ± 4.1
1	30	12.0 ± 5.8
1	45	15.1 ± 10.7 (+35 nm height, 4 number%)
1	60	16.9 ± 12.6 (+40 nm height, 4 number%)
3	2	2.5 ± 0.7
10	2	2.5 ± 0.8 (+10.5 $\pm$ 3.9 nm height, 53 number%)
20	2	11.6 ± 4.2

(Fig. 1C). Fig. 1D shows the mean particle height as a function of silver ion concentration. The produced silver particles were 2.5 and 11.6 nm in size for 3- and 20-mM precursor concentrations, respectively (see Table 1). However, the product from a 10 mM precursor solution was a mixture of 2.5-nm and 10.5-nm particles. As seen, the particle height increased with the precursor concentration.

Silver particles formed after 2- and 3-min irradiation time from the aqueous 1 mM AgNO$_3$ solution were 2.2 ± 0.7 and 3.0 ± 0.9 nm in diameter, respectively (TEM, Fig. 1E). The same particles showed an AFM height of 1.8 ± 0.8 and 2.5 ± 0.6 nm, respectively, indicating spherical shapes. Incidentally, the morphology obtained from the 1-mM AgNO$_3$ solution after 1- and 2-min irradiation indicated clusters of less than 2 nm, approaching the Fermi-wavelength of an electron, that is, de Broglie wavelength at Fermi-levels (~ 0.5 nm for silver).[26–28] Fig. 1F shows the HR-TEM images of the cluster obtained after the irradiation at 2, 3, and 30 min with the 1-mM AgNO$_3$ solution. The lattice fringes on particles at different irradiation times displayed an interplanar spacing of 0.23 nm, ascribed to the (111) plane of silver crystals.[29]

The elemental composition of the produced silver clusters (after 1 min irradiation) was analysed by XPS using an ITO substrate. As seen in the XPS survey spectra, Fig. 2A(a), a peak corresponding to Ag 3d was identified besides those corresponding to ITO (C, O, In and Sn). This result confirms that silver clusters were successfully formed. In a detailed spectrum (Fig. 2A(b)), two peaks with an energy separation of 6.2 eV, at 374.7 eV and 368.5 eV were observed, ascribed to Ag 3d$_{3/2}$ and Ag 3d$_{5/2}$ binding energies, respectively, assigned to metallic silver.[30] The results indicate the formation of metallic silver clusters with no presence of silver oxide nor hydroxide species.

3.2. Characterization of silver quantum particles

The silver particles produced in the absence of reducing agents involves strong reducing species generated when water is exposed to the femtosecond laser light. Based on the mechanism of photolysis of water, a possible reaction is shown in eqn (2):

Fig. 2 (A) XPS (a) survey and fine and deconvoluted spectra of silver clusters after 1 min laser irradiation (b) without scavenger and (c) with OH* scavenger. (B) (a) Survey and (b) Ag 3d fine and deconvoluted peaks of Ag bound to CNF filaments (Ag@CNF filaments). (C) (a) UV-visible absorption, (b) fluorescence excitation and emission spectra and (c) quantum yields at 374 nm excitation of silver particles at different irradiation durations.

$$H_2O + nh\nu \rightarrow e_{aq}^-, H^\star, OH^\star, \textit{etc.} \tag{2}$$
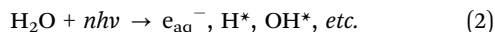
Short-lived solvated electrons e_{aq}^- and hydrogen radicals $H^\star$ are strong reductants, with a redox (standard) potential of $E^0[H_2O/e_{aq}^- = -2.9V_{NHE}$ and $H_2O/H^\star = -2.3V_{NHE}$, respectively].[31] Dissolved metal ions are reduced to their lower oxidation state by the reductants. Meanwhile, hydroxyl radicals $OH^\star$ act as a strong oxidant.[31] Effective scavengers for e_{aq}^-, $H^\star$, and $OH^\star$, such as the TEMPO free radical, 5,5 dimethyl-1-pyrroline N-oxide, and 2-propanol, respectively, were introduced to identify strong reducing species. The silver products formed upon laser irradiation depended on the added scavengers: a TEMPO free radical containing solution produced a smaller number of silver particles (0.05 mg) compared to those in the presence of $H^\star$ (0.12 mg) and $OH^\star$ (0.15 mg) scavengers. Therefore, the solvated electrons e_{aq}^- are confirmed as active species and strong reductants that TEMPO free radicals successfully scavenge. Thus, silver ions are reduced to Ag^0 in a solution following eqn (3).

$$Ag^+ + e_{aq}^- \rightarrow Ag^0 \tag{3}$$

Meanwhile, $OH^\star$ generated during femtosecond laser irradiation forms hydrogen peroxide ($OH^\star + OH^\star = H_2O_2$) that partially oxidizes the product Ag^0, following $2Ag^0 + H_2O_2 = 2Ag^+ + 2OH^-$. When an $OH^\star$ scavenger is added to the precursor solution, the reoxidation reaction is prevented because the generation of $OH^\star$ is inhibited. Thus, the XPS spectrum (Fig. 2A(b)) shows metallic Ag peaks, revealed at 368.8 and 374.8 eV, and an Ag^+ peak at 374.1 eV after the femtosecond laser reaction, and the latter did not appear in the presence of the $OH^\star$ scavenger (Fig. 2A(c)).

The produced clusters were small in size and may generate a symptomatic quantum confinement effect, which results in a discrete electronic structure and molecular behaviors. They included an electronic transition from the highly occupied molecular orbital to lower unoccupied molecular orbital (HOMO–LUMO), enhanced photoluminescence, and others. These behaviors of silver particles are different from those of the silver bulk counterparts, including crystals and nanoparticles. Especially, the optical properties of silver nanoparticles determined by plasmon excitation are associated with the collective nature of the system.[32] Fig. 2C(a) exhibits the UV-visible absorption spectra of the reaction solutions at different irradiation times. It is apparent that the SPR absorption band was absent even after 60-min irradiation.[33] Note that although such absorption is not observed in individual atoms nor in the bulk,[34] conventional silver nanoparticles exhibit a SPR absorption band around 400 nm.[35]

Fig. 2C(b) shows the fluorescence emission and excitation spectra of silver particles produced at different irradiation durations. Silver particles exhibit fluorescence excitation and emission bands at 228 nm and 374 nm, respectively. Generally, quantum-confined materials exhibit size-dependent absorption and fluorescence emission.[35] Since the red shift of the emission band appears due to the increased size, a high energy is necessary to excite the particles and the HOMO–LUMO energy gap may decrease with particle size.[36] However, even at the longest femtosecond laser irradiation time (60 min), the fluorescence properties characteristic of quantum particles still existed though the shift of fluorescence bands was scarce. This result indicates that silver particles formed by the femtosecond laser irradiation (even after 60 min) displayed quantum properties, but those with sizes <17 nm were not enough to induce size-dependent variations in the quantum properties. The quantum efficiency (Φ) of the fluorescent particles was determined by relative methods by using anthracene as a standard (quantum yield = 0.27) in ethanol (refractive index = 1.36). The results (Fig. 2C(c)) confirmed that silver particles exhibited fluorescence but at very low yields (~2%). The absence of the effect of irradiation time was consistent with that of the quantum properties discussed above.

3.3. Catalytic performance of silver particles

4-Nitrophenol, a non-biodegradable organic material found in industrial wastewater, is a highly stable pollutant. It can cause carcinogenic, mutagenic, and other health effects. Fortunately, these effects can be counteracted by the reduction of 4-nitrophenol to 4-aminophenol, a product that is used in the synthesis of analgesic and antipyretic drugs (for instance, paracetamol and phenacetin) and has found uses as a corrosion inhibitor, a photographic developing agent, an anti-corrosion lubricant, and a hair-dying agent.[10]

The catalytic performance of silver particles on the hydrogenation of 4-nitrophenol with $NaBH_4$ was tested as a model reaction. In the presence of $NaBH_4$, the aqueous 4-nitrophenol solution exhibited an absorption band at 400 nm. The pale-yellow solution turned to deep yellow due to the production of 4-nitrophenolate ions. In the absence of the catalyst, the absorption band of 4-nitrophenolate ions remained unchanged even after 110 min (data not shown). This indicates that the hydrogenation of 4-nitrophenol with $NaBH_4$ was not kinetically possible unless the catalysts was absent.[10] More specifically, Fig. 3A(a) depicts the reduction of 4-nitrophenol with $NaBH_4$ in the presence of a silver catalyst. The intensity of the 400 nm band declined with time. Simultaneously, a new band was observed at 301 nm, which increased in intensity. Then the deep yellow color of 4-nitrophenolate ions decreased until becoming colorless.[10,37] The reduction reaction started when the electron transfers from the donor BH_4^- to nitrophenolate ions by the mediation of the silver catalyst. The silver catalyst relays electrons from the electron donor (reductant: BH_4^-) to the acceptor (oxidant: 4-nitrophenolate), effectively reducing 4-nitrophenol to 4-aminophenol.[38] Overall, the silver catalyst was effective in facilitating the hydrogenation of 4-nitrophenol.

The reduction efficiency of the silver catalyst was calculated from the UV-visible absorption spectra using eqn (4):[39]

$$\% \text{ reduction} = ((A_0 - A_t)/A_0) \times 100 \tag{4}$$

where A_0 and A_t are the initial absorbance and the absorbance at time t, respectively. Fig. 3A(b) depicts the percentage of reduction of 4-nitrophenol by silver catalysts with varying sizes. A reduction efficiency higher than 98% was achieved at 6, 12 and 16 min for the Ag catalysts obtained by irradiation at
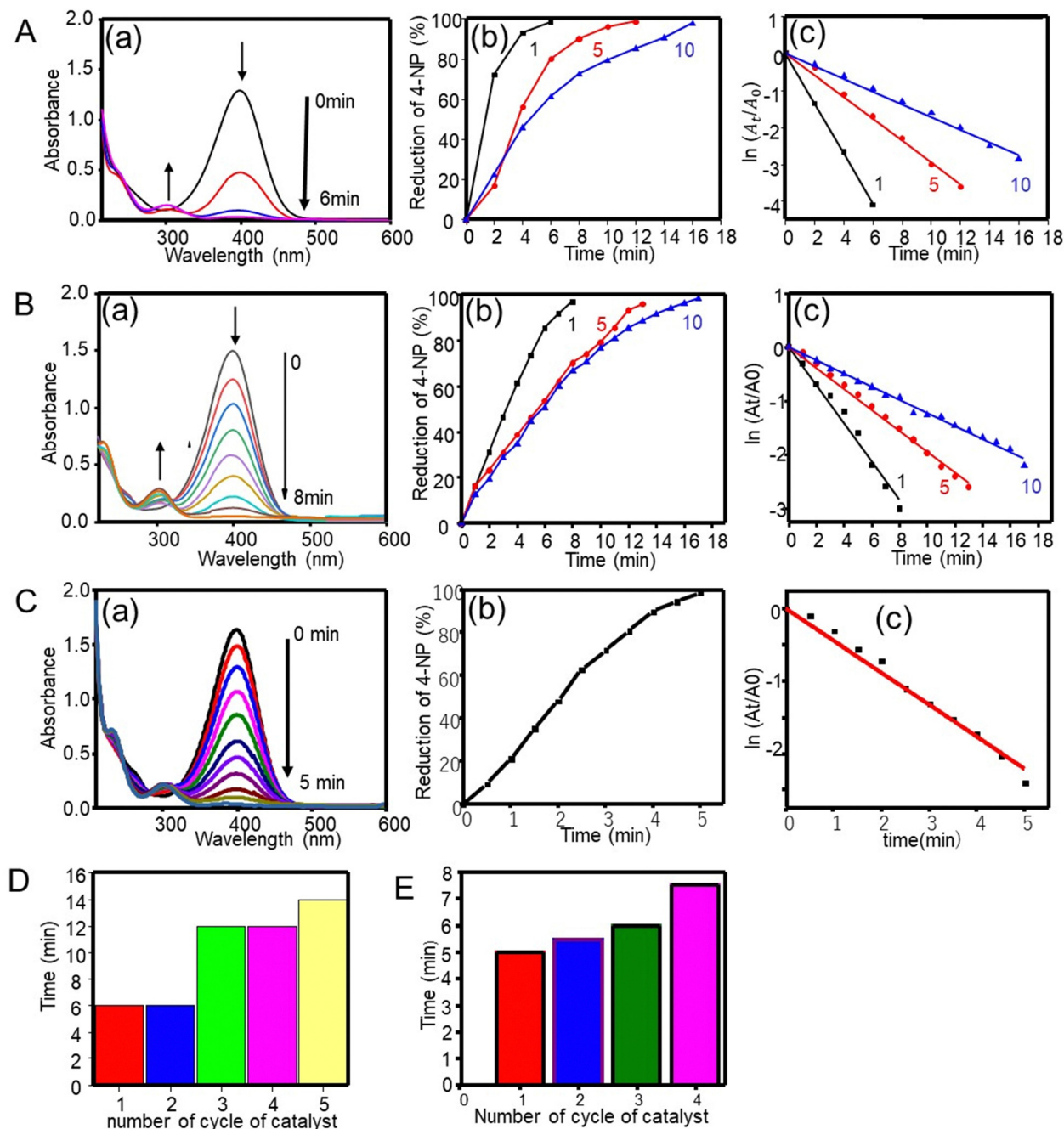
Fig. 3 (A) (a) UV-visible absorption spectra of the hydrogenation reaction of 4-nitrophenol by NaBH$_4$ using a silver catalyst (1-min irradiation): (b) percentage of reduction and (c) ln(A_t/A_0) versus reaction time using different silver catalysts (1, 5 and 10 min irradiation). Corresponding spectra and plots obtained using (B) gold catalysts and (C) the Ag@CNF filament. Recyclability of (D) the silver catalyst (1 min irradiation) and (E) the Ag@CNF filament.

1-min, 5-min and 10-min, respectively. The results indicate that the smaller sized catalysts show better effectivity.

To confirm kinetically the size effect of the catalyst on the relevant reduction reaction, both the zeroth order and the first order kinetics were tested with regard to the 4-nitrophenol concentration: the zeroth order kinetics plot of A_t/A_0 versus time did not follow a linear trend compared to the first order kinetics. The dilute 4-nitrophenol concentration was also adequate to fulfill the condition of the first order kinetics ($KC \ll 1$, where K is the equilibrium constant for adsorption of a reactant onto the

catalyst and C is the concentration of the reactant). Then the apparent rate constant k_{app} was evaluated from the first order reduction reaction equation (eqn (5)),[40] considering that the concentration ratio of the reactant at reaction time t is equivalent to the A_t/A_0 absorbance ratio at a 400 nm band of 4-nitrophenol:

$$\ln \frac{A_t}{A_0} = -k_{app} t \qquad (5)$$

Fig. 3A(c) indicates a good linear fit for $\ln\left(\dfrac{A_t}{A_0}\right)$ as a function of

reaction time (t) for all silver catalysts. The calculated apparent rate constants were 0.676 ($R^2 = 0.999$), 0.294 ($R^2 = 0.997$), and 0.171 ($R^2 = 0.997$) min^{-1} for silver catalysts obtained after 1, 5 and, 10 min irradiation, respectively. The results indicate that the catalyst efficiency improved with the reduced catalyst size. These observations can be rationalized in terms of an increased surface *versus* volume ratio of the catalyst and also by the fact that the particles' surface was bare and with enhanced adsorption of the reactant and reducer (as well as interactions with the catalyst).[41] Compared to the ligand-protected catalysts, unmodified (bare) ones show a better performance. For example, the catalytic reduction of 4-nitrophenol decreases with increasing concentration of the protector (co-polymer ligand) on silver nanoclusters.[11]

The reusability of the silver catalyst (1-min irradiation) for the hydrogenation of 4-nitrophenol was tested by washing the catalyst with water followed by drying. Fig. 3D shows a 98% reduction with time for the silver catalyst, the same as those for the first and second cycles. The reduction efficiency was reduced with further cycles. The possible reason explaining this observation is that the amount of catalyst decreased in each cycle upon washing.

The catalytic properties were further investigated using gold particles prepared *via* the femtosecond irradiation at 1, 5 and 10 min. Fig. 3B(a)–(c) show the UV-visible absorption spectra, the % reduction plot, and the $\ln(A_t/A_0)$ plot. An absorption band at 400 nm decreased with increasing reaction time and finally disappeared at around 6, 12 and 16 min, respectively, indicating that the most effective catalytic performance occurred with gold particles obtained at the shortest irradiation time, that is, with the smaller cluster despite of a smaller amount of used gold catalyst (0.36 mg for 1 min irradiation particle). The importance of the particle size was further revealed by looking at the kinetics of the reaction, which was the first order kinetics with rate constants of 0.356, 0.195 and 0.122 min^{-1} (R^2 of 0.993–0.997) for gold catalysts obtained after 1, 5 and, 10 min irradiation time, respectively.

3.4. Catalytic activity of CNF filaments carrying silver particles (Ag@CNF)

The CNF filaments obtained in this study were ~ 100 μm in diameter (Fig. 4A). The size of the filaments did not change significantly upon loading of silver clusters (Ag@CNF filaments). However, the initially somewhat rough surfaces of the

Fig. 4 (A) A photograph of the CNF filament and FESEM images and EDS spectra of (B) CNF filament and (C) Ag@CNF filament, and (D) the corresponding elemental map of the surface of the Ag@CNF filament.

Table 2 Comparison of catalytic activity of various catalysts for the hydrogenation of 4-nitrophenol

Catalyst[a]	4-Nitrophenol (mM)	NaBH$_4$ (mM)	Size (nm)	Catalyst (mg)	k (min^{-1})	Ref.
AgNC@MIL-101(Fe)	0.2	100	<1	1	0.3144	42
AgNP@CMP	10	1000	3.9	7.5	0.0815	43
CPL-AgNC	0.088	88	3	300	0.91	11
AgNP-chitosan	0.1	10	5	2.1	0.08	44
AgNP@MCNT-polymer	0.1	5	3	10	0.473	45
AgNP@SiNS	0.12	300	2.77	10	0.291	46
AgNC	**0.1**	**100**	**0.9**	**0.52**	**0.676**	[b]
AuNC	**0.1**	**100**	**0.6**	**0.36**	**0.356**	[b]
Ag@CNF	**0.1**	**100**	**—**	**—**	**0.446**	[b]

[a] MIL-101(Fe) = Material Institute Lavoisier, NC = nanocluster, NP = nanoparticle, CPL = copolymer ligand, SiNS = silica nanosheet, and MCNT = multiwalled carbon nanotube. [b] Present work.

filaments became smoother after addition of the silver particles (see Fig. 4B and C). The EDX data of Ag@CNF indicated a silver content of 6.43 wt%. The elemental mapping profile (Fig. 4D) indicated a homogeneous distribution of silver, oxygen and carbon on the surface of the filament.

The XPS survey spectrum of Ag@CNF displays the typical signal corresponding to Ag, while the CNF filament displays only the peaks associated with C and O elements (Fig. 2B). The high-resolution XPS spectrum reveals that the Ag 3d$_{3/2}$ peak can be split into two peaks at 374.9 eV and 376.6 eV, respectively, and the Ag 3d$_{5/2}$ peaks are observed at 369.0 eV and at 370.7 eV. These results provide evidence of the presence of both metallic and ionic silver.[30] The precursor silver cations bind electrostatically with anionic carboxylate groups present on the CNF filament. However, some of the silver ions adsorbed on the CNF filament were not reduced by the femtosecond laser irradiation.

The catalytic activity of the silver nanocluster supported on the CNF filament was examined for the reduction of 4-nitrophenol into 4-aminophenol by NaBH$_4$. As seen in Fig. 3C, the Ag@CNF filament exhibited an absorbance (at 400 nm) that decreased with time, and disappeared after 5 min. The plot of $\ln\left(\dfrac{A_t}{A_0}\right)$ *versus* reaction time t showed a good linear fit with the first-order kinetics (a rate constant of 0.446 min^{-1}). This result indicates that the catalytic efficiency of the Ag@CNF filament was slightly lower than that of free silver cluster catalysts. This effect is likely due to the differences in the stabilization and spatial distribution of the silver clusters attached to the CNF filament. The adsorption of the reactant on the surface of the catalyst and the interactions with the reducer are important. The reduction time increased from 5 min to 7.5 min after reusing the Ag@CNF filaments for 4 cycles (Fig. 3E). Such a reduction in activity was more limited compared to that measured for the free silver clusters (Fig. 3D). All in all, the Ag@CNF catalyst showed better stability than that of the silver clusters.

Table 2 compares the catalytic ability of various catalysts reported in the literature for the hydrogenation of 4-nitrophenol. They include composites or hybrids that protect silver catalysts, based on polymers or inorganic shells. Different relative amounts of the reducer agent compared with the reactant (50–3000 times) were used, as rather small catalysts (1–5 nm). Although the larger catalysts (4 and 5 nm) displayed smaller rate constants, their variation was not necessarily controlled by the catalyst size. Copolymer ligand-bound silver nanoclusters have a high apparent rate constant but required a large amount of catalyst.[11] Despite the larger size (0.9 nm) of the silver clusters compared to the gold counterparts (0.6 nm),[22] the catalytic activity (0.676 min^{-1}) of the former was higher compared to that (0.356 min^{-1}) of the latter. Remarkably, the silver clusters deposited on CNF filaments exhibited low catalytic activity than free silver clusters, but one needs to consider the effective amount of Ag^0 catalyst used in each case: the XRD results indicated the partial reduction of Ag cations on the CNF filaments.

4. Conclusions

In summary, capping-free silver quantum clusters were successfully synthesized by irradiating an aqueous AgNO$_3$ solution with a femtosecond pulse laser. This irradiation technique is different from its conventional laser counterparts, such as femtosecond laser ablation on a solid metal target in an aqueous solution.[47] The excited species produced by the femtosecond pulse laser irradiation were effective reducers in water at room temperature ($\sim$25 °C). Thus, the size of metal products varied with irradiation time, precursor metal ion species, precursor concentration, and laser intensity. By adjusting the irradiation time and precursor concentration for a fixed laser intensity, it was possible to synthesize particles from a 1 mM precursor concentration, with sizes increasing from clusters (<1 nm at 1 min irradiation) to nanoparticles ($\sim$17 nm at 60 min irradiation). The increase of the size with precursor concentration suggests growth that is highly dependent on the tested parameter. The control of the conditions led to the facile synthesis of protector-free metal clusters/nanoparticles. Protector-free silver clusters exhibited photoluminescence (quantum effect) but did not display the plasmonic phenomenon. This is in contrast to conventional silver nanoparticles. An outstanding property of the obtained clusters was their remarkable catalytic efficiency, as demonstrated by the conversion of 4-nitrophenol to 4-aminophenol, which was completed in a short time, within several minutes, compared to that required by conventional nanoparticles.[35] This result is related to their large reactive surface relative to the volume and their available bare surface. The catalytic effect was superior to that observed for gold clusters. Moreover, silver clusters were

effectively bound to filaments produced from cellulose nanofibrils. Overall, this study is expected to open up new opportunities in the fabrication and use of capping-free metallic and quantum clusters, including those bound to filaments, which are demonstrated to show high catalytic activity.

Availability of data and materials

Data and materials in the present work are not available.

Author contributions

SAM and LW: methodology, data acquisition, and visualization. TI and OJR: conceptualization and funding acquisition, writing, and supervision.

Conflicts of interest

The authors declare no competing financial interests or personal relationships that could influence the work reported in this paper.

Acknowledgements

References

1 R. Jin, *Nanoscale*, 2015, **7**(5), 1549–1565.

2 I. Chakraborty and T. Pradeep, *Chem. Rev.*, 2017, **117**(12), 8208–8271.

3 Y. Chen, M. L. Phipps, J. H. Werner, S. Chakraborty and J. S. Martinez, *Acc. Chem. Res.*, 2018, **51**(11), 2756–2763.

4 B. Liu, H. Yao, W. Song, L. Jin, I. M. Mosa, J. F. Rusling, S. L. Suib and J. He, *J. Am. Chem. Soc.*, 2016, **138**(14), 4718–4721.

5 L. Zhang and E. Wang, *Nano Today*, 2014, **9**(1), 132–157.

6 M. A. Ur Rehman, S. Ferraris, W. H. Goldmann, S. Perero, F. E. Bastan, Q. Nawaz, G. G. D. Confiengo, M. Ferraris and A. R. Boccaccini, *ACS Appl. Mater. Interfaces*, 2017, **9**(38), 32489–32497.

7 C. R. Kagan, *Chem. Soc. Rev.*, 2019, **48**(6), 1626–1641.

8 M. Liu and W. Chen, *Nanoscale*, 2013, **5**(24), 12558–12564.

9 K. Shimizu, K. Sawabe and A. Satsuma, *Catal. Sci. Technol.*, 2011, **1**(3), 331–341.

10 W. Zhou, Y. Fang, J. Ren and S. Dong, *Chem. Commun.*, 2019, **55**(3), 373–376.

11 J. Lü, Y. Fu, Y. Song, D. Wang and C. Lü, *RSC Adv.*, 2016, **6**(17), 14247–14252.

12 J. Wilcoxon and B. Abrams, *Chem. Soc. Rev.*, 2006, **35**(11), 1162–1194.

13 H. Hirai, Y. Nakao and N. Toshima, *J. Macromol. Sci., Chem.*, 1978, **12**(8), 1117–1141.

14 W. Tu and H. Liu, *Chem. Mater.*, 2000, **12**(2), 564–567.

15 T. G. Dietz, M. A. Duncan, D. E. Powers and R. E. Smalley, *J. Chem. Phys.*, 1981, **74**(11), 6511–6512.

16 W. Chen, J. Kim, S. Sun and S. Chen, *Phys. Chem. Chem. Phys.*, 2006, **8**(23), 2779–2786.

17 Z. Liu, M. Shamsuzzoha, E. T. Ada, W. M. Reichert and D. E. Nikles, *J. Power Sources*, 2007, **164**(2), 472–480.

18 C. Koenigsmann, W.-P. Zhou, R. R. Adzic, E. Sutter and S. S. Wong, *Nano Lett.*, 2010, **10**(8), 2806–2811.

19 G. F. Gemeda, W.-J. Hwang, T. Imae. and Y.-W. Yen, *J. Colloid Interface Sci.*, 2022, **614**, 310–321.

20 M. B. Getahun, E. B. Santiko, T. Imae, C. L. Chiang and Y. G. Lin, *Appl. Surf. Sci.*, 2022, **604**, 154515.

21 J. Gaol and T. Imae, *J. Environ. Chem. Eng.*, 2023, **11**(6), 111333.

22 T. Imae, A. Rahmawati, A. M. Berhe and M. A. Kebede, *ACS Appl. Nano Mater.*, 2022, **5**(11), 16842–16852.

23 F. J. Rahmania, T. Imae and J. P. Chu, *J. Colloid Interface Sci.*, 2024, **657**, 567–579.

24 L. Wang, M. J. Lundahl, L. G. Greca, A. C. Papageorgiou, M. Borghei and O. J. Rojas, *Sci. Rep.*, 2019, **9**(1), 16691.

25 A. T. R. Williams, S. A. Winfield and J. N. Miller, *Analyst*, 1983, **108**(1290), 1067–1071.

26 B. Han and E. Wang, *Anal. Bioanal. Chem.*, 2012, **402**(1), 129–138.

27 Y. Cao, J. Guo, R. Shi, G. I. N. Waterhouse, J. Pan, Z. Du, Q. Yao, L. Z. Wu, C. H. Tung, J. Xie and T. Zhang, *Nat. Commun.*, 2018, **9**(1), 2379–2385.

28 J. V. Rival, P. Mymoona, K. M. Lakshmi, T. Pradeep and E. S. Shibu, *Small*, 2021, 2005718.

29 M. Tsegay, H. Gebretinsae, J. Sackey, M. Maaza and Z. Nuru, *Mater. Today: Proc.*, 2021, **36**, 368–373.

30 A. Regiel-Futyra, M. Kus-Liśkiewicz, V. Sebastian, S. Irusta, M. Arruebo, A. Kyzioł and G. Stochel, *RSC Adv.*, 2017, **7**(83), 52398–52413.

31 T. Nakamura, H. Magara, Y. Herbani and S. Sato, *Appl. Phys. A: Mater. Sci. Process.*, 2011, **104**(4), 1021–1024.

32 H. Xu and K. S. Suslick, *Adv. Mater. Interfaces*, 2010, **22**(10), 1078–1082.

33 I. Díez and R. H. Ras, *Nanoscale*, 2011, **3**(5), 1963–1970.

34 L. Shang, S. Dong and G. U. Nienhaus, *Nano Today*, 2011, **6**(4), 401–418.

35 P. Díaz-Núñez, J. González-Izquierdo, G. González-Rubio, A. Guerrero-Martínez, A. Rivera, J. M. Perlado, L. Bañares and O. Peña-Rodríguez, *Appl. Sci.*, 2017, **7**(8), 793–803.

36 X. Le Guével, C. Spies, N. Daum, G. Jung and M. Schneider, *Nano Res.*, 2012, **5**(6), 379–387.

37 R. Bendi and T. Imae, *RSC Adv.*, 2013, **3**(37), 16279–16282.

38 A. Gangula, R. Podila, L. Karanam, C. Janardhana and A. M. Rao, *Langmuir*, 2011, **27**(24), 15268–15274.

39 Q. Geng and J. Du, *RSC Adv.*, 2014, **4**(32), 16425–16428.

40 H.-L. Cao, H.-B. Huang, Z. Chen, B. Karadeniz, J. Lü and R. Cao, *ACS Appl. Mater. Interfaces*, 2017, **9**(6), 5231–5236.

41 K. Kuroda, T. Ishida and M. Haruta, *J. Mol. Catal. A: Chem.*, 2009, **298**(1–2), 7–11.

42 D. A. Islam, A. Chakraborty and H. Acharya, *New J. Chem.*, 2016, **40**(8), 6745–6751.

43 H.-L. Cao, H.-B. Huang, Z. Chen, B. Karadeniz, J. Lü and R. Cao, *ACS Appl. Mater. Interfaces*, 2017, **9**(6), 5231–5236.

44 A. Murugadoss and A. Chattopadhyay, *Nanotechnology*, 2007, **19**(1), 015603.

45 S. M. Alshehri, T. Almuqati, N. Almuqati, E. Al-Farraj, N. Alhokbany and T. Ahamad, *Carbohydr. Polym.*, 2016, **151**, 135–143.

46 Z. Yan, L. Fu, X. Zuo and H. Yang, *Appl. Catal., B*, 2018, **226**, 23–30.

47 H. Zeng, X. W. Du, S. C. Singh, S. A. Kulinich, S. Yang, J. He and W. Cai, *Adv. Funct. Mater.*, 2012, **22**(7), 1333–1353.